Coordinated Planning Strategy for Electric Vehicle Charging Stations and Coupled Traffic-Electric Networks

Xu Wang, Mohammad Shahidehpour, *Fellow, IEEE*, Chuanwen Jiang, and Zhiyi Li, *Member, IEEE*

***Abstract*—The proliferation of electric vehicles (EVs) calls for an effective planning of charging stations by coupling the transportation network (TN) with the power distribution network (PDN). This paper conducts an interdisciplinary study on the coordinated planning strategy of EV charging stations in a coupled traffic-electric network. A comprehensive planning model is proposed, which determines the optimal expansion strategies for both TN and PDN, including sites and sizes of new charging stations, charging spots, TN lanes, and PDN lines. In TN, we use an unconstrained traffic assignment model (UTAM) to explicitly capture the steady-state distribution of traffic flows. In PDN, operating conditions are described by a linearized DistFlow. Moreover, EV charging demands and interdependency of TN and PDN are characterized by EV charging station location model. To retrieve a global optimal solution, an equivalent mixed-integer linear programming model with UTAM constraints is formulated for the coordinated planning model. Numerical experiments on coupled traffic-electric networks are conducted to validate the effectiveness of the proposed model and the solution method.**

***Index Terms*—Coordinated planning, charging stations, power distribution network, transportation network, equilibrium.**

NOMENCLATURE

Indices, sets and parameters:

rs	Index for origin-destination (O-D) pair (r, s)
k	Index for paths
i, j	Index for nodes in transportation network (TN) or nodes in power distribution network (PDN)
(i, j)	Index for distribution line from i to j in PDN
$\mathbf{OD}$	Set of all O-D pairs
$\mathbf{K_{rs}}$	Set of paths for O-D pair (r, s)
$\mathbf{T_N}$	Set of nodes (intersections or zones) in TN
$\mathbf{T_A}$	Set of links (arcs or roads) in TN
$\mathbf{\Gamma_k^{-1}}/\mathbf{\Gamma_k}$	Set of successor/predecessor links on path k
$\mathbf{\Gamma_k^r}/\mathbf{\Gamma_k^s}$	Set of origin/destination links on path k
$\mathbf{L_k}$	Set of links on path k in TN
$\mathbf{D_N}$	Set of electrical nodes in PDN
$\mathbf{D_A}$	Set of distribution lines in PDN
c_a	Flow capacity of link a in TN
t_a	Travel time on link a in TN
q_{rs}	Traffic flow demand between O-D pair (r, s)
δ_{ak}^{rs}	If path k from O-D pair (r, s) contains link a; otherwise, $\delta_{ak}^{rs} = 0$.
$c_{1,a}$	Construction cost for new charging station at link a
$c_{2,a}$	Cost for adding an extra charging spot at link a
$c_{3,a}$	Per-unit cost for a new expanded lane at link a
c_{ij}	Per-unit cost for an extra distribution line (i, j)
$c_{4,a}$	Cost for substation capacity expansion at link a
ω	Monetary value of travel time
$\bar{y}_a$	Maximum number of charging spots in station a
$g(y_a)$	Charging service ability function
d_a	Distance of link a in TN
R	Driving range of EVs with full charge
SOC_O	Arrival *SOC* of an EV at the origin nodes
SOC_D	Departure *SOC* of an EV at the destination nodes
x_{ij}/r_{ij}	Reactance/resistance of distribution line (i, j)
P_i/Q_i	Active and reactive power demand at node i in PDN
η	Charging rate of traffic flow in TN
$\bar{v}_i/\underline{v}_i$	Upper/lower bound of voltage magnitude at node i
$\bar{p}_{ij}$	Active power flow capacity of distribution line (i, j)
N_a^c	Upper bound number of lanes expanded on link a
N_{ij}	Upper bound number of distribution lines built in parallel with existing distribution line (i, j)

Variables:

x_a	Aggregated traffic flow on link a
y_a	Positive integer variable, number of charging spots invested in station at link a
s_a	Binary variable indicating charging station located at link a (1) or not (0)
n_a^c	Integer variable, number of lanes expanded at link a

Manuscript received November 23, 2017; revised March 26, 2018 and July 7, 2018; accepted August 19, 2018. Date of publication August 24, 2018; date of current version December 19, 2018. This work was supported in part by the China Postdoctoral Science Foundation under Grant 2017M611562, and in part by the National Natural Science Foundation of China under Grant 51577116. Paper no. TPWRS-01770-2017. *(Corresponding author: Mohammad Shahidehpour.)*

X. Wang is with the School of Electronic Information and Electrical Engineering, Shanghai Jiao Tong University, Shanghai 200240 China, and also with the Galvin Center for Electricity Innovation, Illinois Institute of Technology, Chicago, IL 60616 USA (e-mail: wangxu1989@sjtu.edu.cn).

M. Shahidehpour is with the Galvin Center for Electricity Innovation, Illinois Institute of Technology, Chicago, IL 60616 USA, and also with the Renewable Energy Research Group, King Abdulaziz University, Jeddah 21589, Saudi Arabia (e-mail: ms@iit.edu).

C. Jiang is with the School of Electronic Information and Electrical Engineering, Shanghai Jiao Tong University, Shanghai 200240 China (e-mail: jiangcw@sjtu.edu.cn).

Z. Li is with the Galvin Center for Electricity Innovation, Illinois Institute of Technology, Chicago, IL 60616 USA (e-mail: zli132@hawk.iit.edu).

Color versions of one or more of the figures in this paper are available online at http://ieeexplore.ieee.org.

Digital Object Identifier 10.1109/TPWRS.2018.2867176

0885-8950 © 2018 IEEE. Personal use is permitted, but republication/redistribution requires IEEE permission.
See http://www.ieee.org/publications_standards/publications/rights/index.html for more information.

Authorized licensed use limited to: Washington State University. Downloaded on April 22,2021 at 20:11:05 UTC from IEEE Xplore. Restrictions apply.

SOC_O^k State-of-charge of EV leaving charging station on link *a* on path *k*
f_k^{rs} Traffic flow on path k between O-D pair (*r*, *s*)
p_{ij}/q_{ij} Active/reactive power flow on distribution line (*i*, *j*)
v_i Voltage magnitude at node *i* in PDN
n_{ij} Integer variable, number of distribution lines built in parallel with existing distribution line (*i*, *j*)

I. Introduction

ELECTRIC VEHICLES (EVs) have been widely regarded a promising alternative for instituting energy sustainability and combating climate change [1]. The rapid deployment of EVs has introduced an emerging mandate for coupling transportation network (TN) with power distribution network (PDN) [2]–[4], which could enhance the planning and the operation of charging stations.

When considering charging stations, economic and security constraints of PDN are usually critical for minimizing investment costs on upgrading power systems. In [5], a two-stage procedure was developed for planning EV charging stations in PDN, where the first stage determined locations of charging stations and the second stage calculated their optimal capacity by a modified primal-dual interior point method. Reference [6] presented a basic framework for the planning of EV charging/swap stations based on life cycle cost analyses. However, transportation constraints were ignored in [5], [6] and corresponding results would need to be readjusted based on TN practical data. Moreover, a multi-objective coordinated planning model was presented in [7] for integrated power distribution and EV charging systems. The model incorporated the user equilibrium (UE) based traffic assignment model to capture the distribution of traffic flow in the TN. Recently, coordinated planning for EV charging stations and PDN infrastructures has been addressed in [8] and [9]. However, few publications have involved the coordinated planning for EV charging stations in PDN and road capacity expansion in TN with traffic flow equilibrium constraints.

Considering the TN perspective, managing the distribution of vehicular flow is the main concern. An integrated planning framework for the optimal siting and sizing of EV charging stations in an urban area is proposed in [10], where spatial and temporal charging demands are generated by a forecasting method and the effect of traffic flow on EV charging demand is ignored. In this regard, the authors in [11] use real world and comprehensive individual travel survey data to simulate the TN traffic flow distribution in which EV charging demands are estimated more accurately. However, the detail survey data may not be readily available for other practical applications.

Considering the EV mobility, a constrained flow-refueling location model is proposed in [12], which seeks optimal locations of TN charging stations. In this model, EV charging demands are estimated by considering the traffic in origin-destination (O-D) pairs. However, a detailed traffic assignment model describing TN flow distributions is ignored in [10]–[12]. Incorporating topological dynamics of TN and EV route choices with limited driving ranges, a multi-period multi-path model for EV charging stations is proposed in [13]. The road network expansion planning is a classic TN problem, which is formulated as a bi-level mathematical program with traffic flow equilibrium constraints [14]. Also, the coordinated expansion planning of road capacity and on-road EV charging stations has attracted increasing attentions in recent years but the published work on this issue is limited. In addition, the coordinated planning of coupled traffic-electric networks has been the focus of several studies in recent years.

Moreover, there are recent papers with interdisciplinary studies on the coupled traffic-electric network. Considering the interdependent TN and PDN, [15] identified the coupled network equilibrium by iteratively solving the traffic assignment problem and the optimal power flow problem. To calculate the optimal coordinated operation of the coupled TN and PDN, a mixed-integer second-order cone program with traffic UE constraints was formulated in [16]. A two-stage stochastic programming model is proposed in [17] for solving the jointly planning problem of EV charging stations and distributed photovoltaic power plants in the coupled TN and PDN. In addition, [18] studied the system-level effects on EV battery charging in a coupled power and transportation networks, considering spatial variations in electricity prices caused by power grid congestion [18]. In [19], the authors solved the hourly security-constrained unit commitment with vehicle routing problem in a coupled railway transportation network and power grid. Reference [20] provided a reliability assessment method for coupled transportation and electrical power systems with EVs. Moreover, resilience enhancement strategies for the coupled PDN and urban TN were given in [21]. References [15]–[21] involved optimal operation, coordinated planning, reliability assessment and resilience enhancement problems in a coupled transportation and power system. In the coordinated planning problem, publications did not focus on optimal expansion strategies for both TN and PDN with traffic UE constraints, including sites and sizes of new charging stations, charging spots, TN lanes and PDN lines.

Consequently, this paper aims to comprehensively address the coordinated planning problem for both EV charging stations and coupled traffic-electric networks. The major innovations of this paper are in three aspects:

1) The unconstrained traffic assignment model (UTAM) is proposed in which road capacity constraints are relaxed and TN traffic flow equilibrium constraints are considered for the road capacity expansion. UTAM utilizes the Nesterov & de Palma (NdP) model [22]–[24] and primal-dual optimality conditions [25] for calculating the TN traffic flows, which overcome the non-convexity of conventional Bureau of Public Road (BPR) function [26] when road capacity is a variable.
2) An EV charging station location model (ECSLM) is introduced, in which constraints on EV driving range and traffic flow equilibrium are explicitly incorporated. ECSLM utilizes driving range logics to determine candidate locations for EV charging stations and adopts a linear function to model the serviceability of EV charging stations in TN.
3) A mixed-integer linear programming (MILP) model for the coordinated planning of coupled traffic-electric networks is formulated, which could find the global optimal solution with a reasonable computation effort for moderately sized networks. The constrained-planning

Authorized licensed use limited to: Washington State University. Downloaded on April 22,2021 at 20:11:05 UTC from IEEE Xplore. Restrictions apply.

model optimizes the total cost for the construction of charging stations, vehicle travel time, and expansion of PDN and TN.

II. Formulation of Coupled Traffic-Electric Networks

A. Unconstrained Traffic Assignment Model

A brief introduction to models and methods applied to the traffic assignment problem (TAP) in TN is presented.

Consider a strongly connected TN which is represented by $\mathbf{G_T} = [\mathbf{T_N}, \mathbf{T_A}]$, where $\mathbf{T_N}$ is the set of nodes (i.e., intersections or zones) and $\mathbf{T_A}$ is the set of links (i.e., arcs or roads). Each link $a \in \mathbf{T_A}$ has a traffic flow capacity c_a (i.e., maximum number of vehicles that can cross link $a \in \mathbf{T_A}$ per unit time) and a free travel time t_a^0 (i.e., travel time across link $a \in \mathbf{T_A}$ at the speed limit without causing congestion) [2].

For each O-D pair (*r*, *s*) connected by a set of paths $\mathbf{K_{rs}}$, there are q_{rs} traffic flow demands. Links are the edges of $\mathbf{T_N}$ graph. Paths refer to all possible paths between an origin node and a destination node of a $\mathbf{T_N}$ graph. We denote traffic flows on link $a \in \mathbf{T_A}$ and path $k \in \mathbf{K_{rs}}$ by x_a and f_k^{rs}, respectively. For O-D pair (*r*, *s*), the traffic flow on path $k \in \mathbf{K_{rs}}$ is f_k^{rs}. If the link $a \in \mathbf{T_A}$ belongs to the path $k \in \mathbf{K_{rs}}$, the traffic flow on that link for the O-D pair (*r*, *s*) is f_k^{rs}. The total traffic flow on that link for all O-D pairs is $x_a = \sum_{rs} \sum_k f_k^{rs} \delta_{ak}^{rs}$. Here, variable indicator $\delta_{ak}^{rs} = 1$ if the path *k* on O-D pair (*r*,*s*) contains link *a*; otherwise, $\delta_{ak}^{rs} = 0$.

Associated with each link $a \in \mathbf{T_A}$ is a travel time function $t_a(x_a)$, which provides the travel time on link *a* as a function of x_a. Due to congestion, $t_a(x_a)$ is a strictly monotonically non-decreasing function [2], [25]–[27]. There are many functions that describe the relationship between the travel time and link parameters (e.g., link traffic flow, road capacity, link free travel time, etc.). Among them, the widely used BPR function [2], [26] is shown as follows:

$$t_a(x_a) = t_a^0 \left[1 + 0.15\left(\frac{x_a}{c_a}\right)^4\right], \forall a \in T_A \tag{1}$$

The road capacity c_a is a decision variable in the road expansion planning problem, which makes (1) a non-convex function. Hence, the NdP model and primal-dual optimality conditions are utilized to overcome the non-convexity. The NdP model [22]–[24] is used to determine the TN utilization, which is briefly introduced as follows.

1) *Assumptions in NdP Model:* We elaborate on two concepts in static TAP, i.e., UE and social optimum (SO).
   a) UE (first Wardrop principle) [28]: Each driver selects his fastest route. In the UE pattern, no driver can unilaterally change its current route to reduce travel time.
   b) SO (second Wardrop principle) [28]: The total travel time (i.e., sum of all drivers' travel time) is minimized. In the SO pattern, every driver must select his route cooperatively to guarantee the most efficient TN utilization.

Obviously, SO is an ideal traffic assignment pattern which lacks practical applications. Hence, we adopt UE in the coordinated planning of a traffic-electric system since it is more practical and captures the selfish behavior of drivers.

The link travel time function $t_a(x_a)$ plays an important role in a TAP model. Two more weak assumptions are made by Nesterov and de Palma in [23] to mitigate the discrepancy caused by the link travel time function. Using [25], further assumptions for the TN in UE pattern are made as follows:

Assumption 1: In the UE pattern, the traffic flow x_a on link *a* never exceeds the link capacity c_a, i.e., $x_a \le c_a$.

Assumption 2: In the UE pattern under Assumption 1, the travel time t_a on link *a* is equal to its free travel time t_a^0 when the traffic flow x_a is below its capacity c_a; the travel time t_a is equal to its free travel time plus a delay penalty λ_a^* when x_a reaches its capacity c_a, i.e.,

$$t_a = \begin{cases} t_a^0, & x_a < c_a \\ t_a^0 + \lambda_a^*, & x_a = c_a \end{cases} \tag{2}$$

where λ_a^* is a delay penalty for link *a* which is equal to the value of the dual variable of link capacity (7). Different from the BPR function (1), the link travel time function in the NdP model is convex. The total travel time is defined as $\sum_{a \in T_A} x_a t_a$.

2) *NdP Model:* Based on the above assumptions, TAP at the SO pattern with no delays (i.e., $t_a = t_a^0$) is solved as follows [25], [29]:

$$[\text{NdP} - \text{SO}] \quad \min_{x_a, t_a, f_k^{rs}} \sum_{a \in T_A} x_a t_a = \min_{x_a, f_k^{rs}} \sum_{a \in T_A} x_a t_a^0 \tag{3}$$

$$\text{s.t.} \quad \sum_k f_k^{rs} = q_{rs}, k \in \mathbf{K_{rs}}, (r,s) \in \mathbf{OD} \qquad [\pi_{rs}] \tag{4}$$

$$\sum_{rs} \sum_k f_k^{rs} \delta_{ak}^{rs} = x_a, (r,s) \in \mathbf{OD}, \quad k \in \mathbf{K_{rs}}, a \in \mathbf{T_A} \quad [\mu_a] \tag{5}$$

$$f_k^{rs} \ge 0, (r,s) \in \mathbf{OD}, k \in \mathbf{K_{rs}} \tag{6}$$

$$x_a \le c_a, a \in \mathbf{T_A} \qquad [\lambda_a] \tag{7}$$

Here, variable indicator $\delta_{ak}^{rs} = 1$ if path *k* from O-D pair (*r*, *s*) contains link *a*; otherwise, $\delta_{ak}^{rs} = 0$. π_{rs}, μ_a and λ_a are dual variables of (4), (5) and (7), respectively. The objective function (3) corresponds to the total travel time with no delays. Constraints (4)–(6) satisfy the traffic flow demand between each O-D pair. Constraint (7) is the link capacity limit indicating that no congestion can happen in the SO pattern. However, (4)–(7) may be violated in certain traffic congestion cases which make [NdP-SO] infeasible.

Hence, Nesterov and de Palma [23] take dual variables of the link capacity (7) as a delay penalty for links that are at capacity limit. Below is the detailed introduction.

3) *Lagrange relaxation:* We associate (7) to a dual variable $\lambda_a, \forall a \in T_A$. Relaxing (7), the Lagrange dual problem is

Authorized licensed use limited to: Washington State University. Downloaded on April 22,2021 at 20:11:05 UTC from IEEE Xplore. Restrictions apply.

formulated as:

$$[\mathrm{NdP-LD}] \quad \max_{\lambda_a \geq 0} \min_{x_a, f_k^{rs}} \left\{ \sum_{a \in T_A} \left[x_a t_a^0 + \lambda_a (x_a - c_a) \right] \middle| \times \text{s.t. } (4)-(6) \right\} \tag{8}$$

For fixed $\lambda_a^0 \geq 0$ and each $(r, s) \in \mathbf{OD}$, the above NdP-LD problem is converted into the following linear problem (LP):

$$[\mathrm{NdP-LP}] \quad \min_{f_k^{rs}} \left\{ \sum_a \left[\sum_k f_k^{rs} \delta_{ak}^{rs} (t_a^0 + \lambda_a^0) - \lambda_a^0 c_a \right] \right\} \tag{9}$$

$$\sum_k f_k^{rs} = q_{rs}, f_k^{rs} \geq 0, a \in \mathbf{T_A}, k \in \mathbf{K_{rs}} \tag{10}$$

Equations (9)–(10) establish a NdP-LP model without capacity constraints, where the objective function (9) corresponds to the total travel time $t_a = t_a^0 + \lambda_a^0$ for assigning drivers in O-D pair (*r*, *s*). We suppose the optimal solution of NdP-SO is x_a^* and the corresponding Lagrange dual multiplier of (7) is λ_a^*.

According to [22]–[25], as the strong duality holds for linear program, (x_a^*, t_a^0) is a traffic assignment at SO and $(x_a^*, t_a^0 + \lambda_a^*)$ is a traffic assignment at UE.

Without capacity constraints, SO and UE give the same traffic assignments which only differ in travel time and Lagrange multipliers λ_a^* are incentives for selfish drivers to reach SO. Accordingly, the UTAM formulation using the primal-dual optimality condition of NdP-SO is given as:

$$[\mathrm{UTAM}] \quad \min \sum_a \sum_k f_k^{rs} \delta_{ak}^{rs} (t_a^0 + \lambda_a) \tag{11}$$

$$\text{s.t.} \quad \sum_k f_k^{rs} - q_{rs} = 0, \sum_k f_k^{rs} \delta_{ak}^{rs} - c_a \leq 0, f_k^{rs} \geq 0 \tag{12}$$

$$\lambda_a \geq 0, \mu_a - \lambda_a = t_a^0, \pi_{rs} - \sum_a \sum_k \delta_{ak}^{rs} \mu_a \leq 0 \tag{13}$$

$$\sum_{rs} \pi_{rs} q_{rs} - \sum_a \lambda_a c_a = \sum_{rs} \sum_a \sum_k f_k^{rs} \delta_{ak}^{rs} t_a^0 \tag{14}$$

$$a \in \mathbf{T_A}, k \in \mathbf{K_{rs}}, rs \in \mathbf{OD} \tag{15}$$

where (12) and (13) represent feasible region constraints of primal and dual variables, respectively; (14) represents the strong duality condition for NdP-SO. Since NdP-SO is an LP, the primal-dual optimality condition provides its optimal solution. Therefore, (12)–(15) is the traffic assignment at UE which determines λ_a. The only difference between NdP-SO and UTAM is that the latter objective function has one more item, i.e., $\sum_a \sum_k f_k^{rs} \delta_{ak}^{rs} \lambda_a$. As both f_k^{rs} and λ_a are determined by (12)–(15), λ_a can be replaced by the optimal Lagrange multipliers λ_a^* and the objective function of UTAM is linear. In this paper, we first obtain the values of f_k^{rs} and λ_a using (12)–(15), and then calculate the objective function. In addition, c_a is a parameter representing the flow capacity of link *a* in UTAM. Therefore, UTAM is a linear programming model, given the values of λ_a^* and c_a.

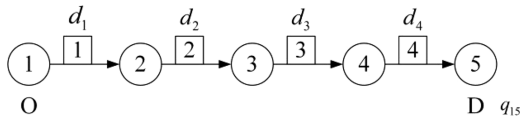

Fig. 1. Driving range logic schematic.

B. EV Charging Station Location Model

We present ECSLM here, which is inspired by the mathematical formulation of capacitated-flow refueling location model (CFRLM) [12]. Compared with CFRLM, the proposed ECSLM offers two advantages. First, ECSLM applies UTAM to capture the steady-state distribution of TN traffic flows at UE for different road expansion strategies. This application offers a practical model for the coordinated planning of coupled traffic-electric networks because road capacity is relevant to the TN traffic flow distribution of EVs, which determines the PDN charging demand. However, road capacity expansion, total travel time of vehicles and traffic flow distribution are not involved in CFRLM. Second, instead of constructing the expanded network in CFRLM, detailed mathematical constraints for driving range logic are provided in ECSLM. In CFRLM, one must construct the expanded network before solving the problem which is a time consuming work when the transportation network is large and complex. This step could be omitted in ECSLM.

We first review the driving range logic [29] and then provide the relevant mathematical formulation. Consider a TN graph $\mathbf{G_T} = [\mathbf{T_N}, \mathbf{T_A}]$ in Fig. 1, with a single path *k* between O-D pair (1, 5), i.e., {link1→link2→link3→link4}. The path *k* has 5 TN nodes, i.e., $\mathbf{T_N} = \{1, 2, 3, 4, 5\}$, and 4 links, i.e., $\mathbf{T_A} = \{\text{link1, link2, link3, link4}\}$, with link distance d_1, d_2, d_3 and d_4, respectively. A flow demand representing EVs between O-D pair (1,5), i.e., q_{15}, with driving range *R* (km) would travel from the origin node 1 to the destination node 5 with a single charge. We assume EVs enter TN at the origin node with *SOC* equal to SOC_O and leave TN at the destination node 5 with *SOC* higher than SOC_D. *SOC* of EVs after charging is assumed to be 1. Network planner aims to locate EV charging stations in the candidate location set T_A (midpoint of link *a*, which can be extended by adding auxiliary nodes on individual links with pre-set distances) to supply EVs.

Generally, driving range logic constraints follow two stated rules. The first rule is that the distance between two charging stations has to be smaller than the driving range *R*. The second rule constrains the EV's *SOC* at origin and destination nodes. We assume there are no charging stations at origin and destination nodes. Specifically, EV's charging level at the origin node is SOC_O so that it can reach the first charging station. Similarly, the location of the last charging station on path *k* should not be far from the destination node so that an EV can leave TN with an *SOC* that is higher than SOC_D. Mathematically, we obtain the following TN constraints shown in Fig. 1:

$$SOC_O - 0.5d_1/R \geq 0 \tag{16}$$

$$SOC_1 = SOC_O - 0.5d_1/R + s_1(1 - SOC_O + 0.5d_1/R) \tag{17}$$

Authorized licensed use limited to: Washington State University. Downloaded on April 22,2021 at 20:11:05 UTC from IEEE Xplore. Restrictions apply.

$$SOC_{a+1} = SOC_a - 0.5(d_a + d_{a+1})/R + s_{a+1}\left[1 - SOC_a + 0.5(d_a + d_{a+1})/R\right], a = 1, 2, 3 \quad (18)$$

$$SOC_a \geq 0, a = 1, 2, 3, 4 \quad (19)$$

$$SOC_4 - 0.5d_4/R \geq SOC_D \quad (20)$$

Since the candidate location of EV charging station is set at the midpoint of link a, $0.5d_a$ and $0.5(d_a + d_{a+1})$ $(a = 1, 2, 3, 4)$ in (16)–(20) represent the distance between two candidate locations of EV charging stations. Equation (16) ensures an EV at origin node can reach the first candidate location of EV charging station. Similarly, (20) indicates that an EV arrives at the destination node with a required *SOC* that is higher than SOC_D. Equations (17) and (18) present the *SOC*s of an EV traversing through candidate locations of EV charging stations. Equation (19) demonstrates that an EV can travel through all candidate locations of EV charging stations along the paths located between a certain O-D pair, with its SOC_a higher than or equal to 0.

Accordingly, the driving range logic constraints for path k between a certain O-D pair are generalized as follows:

$$SOC_O - 0.5d_a/R \geq 0, a \in \mathbf{\Gamma_k^r}, k \in \mathbf{K_{rs}} \quad (21)$$

$$SOC_a^k = SOC_O - d_a/2R + s_a(1 - SOC_O + d_a/2R), \quad a \in \mathbf{\Gamma_k^r}, k \in \mathbf{K_{rs}} \quad (22)$$

$$SOC_b^k = SOC_a^k - \frac{d_a + d_b}{2R} + s_b\left(1 - SOC_a^k + \frac{d_a + d_b}{2R}\right), \quad a \in \mathbf{\Gamma_k^{-1}}, b \in \mathbf{\Gamma_k}, k \in \mathbf{K_{rs}} \quad (23)$$

$$SOC_a^k \geq 0, a \in \mathbf{L_k}, k \in \mathbf{K_{rs}} \quad (24)$$

$$SOC_a^k - 0.5d_a/R \geq SOC_D, a \in \mathbf{\Gamma_k^s}, k \in \mathbf{K_{rs}} \quad (25)$$

Then, ECSLM is formulated as follows:

$$\min_{s_a, y_a, f_k^{rs}} \left\{ \sum_a (c_{1,a}s_a + c_{2,a}y_a) + \omega \sum_a \sum_k f_k^{rs}\delta_{ak}^{rs}(t_a^0 + \lambda_a^*) \right\} \quad (26)$$

$$\text{s.t.} \quad \arg\min_{f_k^{rs}} \left\{ \sum_a \sum_k f_k^{rs}\delta_{ak}^{rs}(t_a^0 + \lambda_a^*) \middle| (12)-(15) \right\} \quad (27)$$

$$\text{Driving range logic constraints } (21)-(25) \quad (28)$$

$$y_a \leq \bar{y}_a s_a \quad (29)$$

$$\eta \sum_k f_k^{rs}\delta_{ak}^{rs} \leq g(y_a), a \in \mathbf{T_A}, k \in \mathbf{K_{rs}} \quad (30)$$

The first term in (26) is the total investment cost for EV charging stations, including the costs of station constructions and charging spot installations. The second term in (26) is the monetary cost of travel time, which is proportional to the total vehicle travel time in the UE pattern. Equation (27) defines the UE traffic flow constraints, which determine the total vehicle travel time using UE and the TN traffic flow distribution. Equation (28) constrains driving range logic for feasible locations of EV charging stations. Equation (29) gives the upper-bound of the number of charging spots in a charging station.

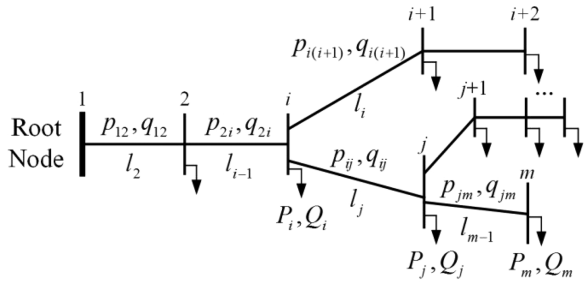

Fig. 2. A typical radial PDN.

Equation (30) is the serviceability constraint for each charging station, which is a function of the number of charging spots [30]. For simplicity, we assume a linear relationship $g(y_a) = \mathrm{A}y_a + \mathrm{B}$ in our case study, in which $\mathrm{A} = 3$ and $\mathrm{B} = 4$.

C. Distribution Network Model With EV Charging Demand

The EV charging stations located in TN are served by a PDN. Consider a connected graph $\mathbf{G_D} = [\mathbf{D_N}, \mathbf{D_A}]$, where $\mathbf{D_N}$ and $\mathbf{D_A}$ are sets of PDN nodes and lines, respectively. Unlike meshed transmission networks, a PDN is operated with a radial topology. Consequently, DistFlow [31] is applied to calculate PDN power flow and voltage profile. Fig. 2 depicts a typical radial PDN, which consists of *n* nodes and *n*-1 branches. The nodes are numbered in descending order. In case a branch is located between *i*-th and (*i*+1)-th nodes of the radial network, the line number would be the downstream node number minus one.

For any node *j* and any distribution line (*i*, *j*) in Fig. 2, the DistFlow equations are defined as

$$\sum_{n|(j,n)\in\mathbf{L}} p_{jn} = p_{ij} - r_{ij}(p_{ij}^2 + q_{ij}^2)/v_j^2 - P_j, j \in \mathbf{D_N}, \times (i,j) \in \mathbf{D_A} \quad (31)$$

$$\sum_{n|(j,n)\in\mathbf{L}} q_{jn} = q_{ij} - x_{ij}(p_{ij}^2 + q_{ij}^2)/v_j^2 - Q_j, j \in \mathbf{D_N}, \times (i,j) \in \mathbf{D_A} \quad (32)$$

$$v_j^2 = v_i^2 - 2(r_{ij}p_{ij} + x_{ij}q_{ij}) + (r_{ij}^2 + x_{ij}^2)\left(\frac{p_{ij}^2 + q_{ij}^2}{v_i^2}\right), \times (i,j) \in \mathbf{D_A} \quad (33)$$

In the above equations, *i* is the root node of *j* and $(j, n) \in \mathbf{D_A}$ is the set of distribution lines that flow out of node *j*, i.e., *n* is the set of descendant nodes of *j*. Ignoring the loss terms in (31) and (32), the linearized power balance is stated as

$$\sum_{n|(j,n)\in\mathbf{L}} p_{jn} = p_{ij} - P_j, j \in \mathbf{D_N}, (i,j) \in \mathbf{D_A} \quad (34)$$

$$\sum_{n|(j,n)\in\mathbf{L}} q_{jn} = q_{ij} - Q_j, j \in \mathbf{D_N}, (i,j) \in \mathbf{D_A} \quad (35)$$

The third term on the right-hand side of (33) is much smaller than the second term which can be ignored. Moreover, $(v_i - v_1)^2 \approx 0$, i.e., $v_i^2 + v_1^2 - 2v_iv_1 \approx 0$, in a radial PDN

Authorized licensed use limited to: Washington State University. Downloaded on April 22,2021 at 20:11:05 UTC from IEEE Xplore. Restrictions apply.

because the voltage magnitude at each node is close to that of reference node v_1. Substituting in (33), we obtain

$$v_j = v_i - (r_{ij}p_{ij} + x_{ij}q_{ij})/v_1, (i,j) \in \mathbf{D_A} \tag{36}$$

The linearized DisFlow (34)–(36) are considered in our coordinated planning.

For traffic-electric networks, each PDN node serves its load with conventional resources and EV charging request (if exists), which is assumed to be a linear function of traffic flow with a pre-determined charging rate η. The applications in [32], [33] illustrate that the above assumption is reasonable for coupled traffic-electric networks. The interface between TN and PDN is expressed as:

$$P_i = P_i^d + \eta \sum_{a \in C(i)} s_a x_a, i \in \mathbf{D_N} \tag{37}$$

where *C*(*i*) represents the set of charging stations on link *a* in TN that are served by node *i* in PDN; P_i^d is the traditional constant demand at node *i* in PDN.

III. Coordinated Planning Model For Coupled Traffic-Electric Networks

A. Coordinated Planning Model

Some of the basic variables in the coordinated planning of coupled traffic-electric networks are presented as follows:

1) New lanes which are numbered as $n_a^c \le N_a^c, a \in \mathbf{T_A}$ are expanded in parallel with existing links. Each expanded lane has the same capacity which is a linear function of the original link capacity, i.e., $\Delta c_a = \omega_c c_a^0$ $(\omega_c = 0.5)$, where c_a^0 is the original link capacity. In a lane expansion, a single lane is added in a one-way road and two lanes are added in a two-way road.
2) New EV charging stations are added at midpoint (can also be extended to pre-defined candidate locations) of link *a*. Decision to build an EV charging station at link *a* is represented by a binary variable s_a, which satisfies the driving range logic constraints.
3) New charging spots are added in an EV charging station at link *a*, which determines the charging serviceability. The number of spots is given by a positive integer variable y_a, which is optimized according to the traffic flow of link *a*.
4) New distribution lines are added in parallel with existing distribution lines. The number n_{ij} is determined by the maximum active power flow on distribution line (*i, j*). Each new distribution line between nodes *i* and *j* is represented by the same set of parameters. Compared with the original values, resistances and reactances are reduced to 1 $(1 + n_{ij})$ and the maximum active power flow is stated as $(1 + n_{ij})\bar{p}_{ij}$.

With given both traffic and power demand, the coordinated planning model, following [25] for a coupled traffic-electric network, is presented as:

$$\min_{s_a, y_a, n_a^c} \quad C_{TN} + C_{PDN} \tag{38}$$

$$\text{s.t.} \quad Cons - \text{TN}; Cons - \text{PDN} \tag{39}$$

B. Coordinated Planning Objective

The coordinated planning model is to minimize investment costs in both TN and PDN. The first term C_{TN} in (38) is the investment cost in TN,

$$C_{TN} = \sum_{a \in \mathbf{T_A}} \left[(c_{1,a}s_a + c_{2,a}y_a + c_{3,a}n_a^c) + \omega(t_a^0 + \lambda_a)x_a \right] \tag{40}$$

where the first term in C_{TN} represents the investment cost of new EV charging stations, charging spots and lanes; the second term is the equivalent travel cost in the UE pattern.

The second term in (38) is the investment cost in PDN,

$$C_{PDN} = \sum_{(i,j) \in \mathbf{D_A}} c_{ij}n_{ij} + \sum_{a \in C(i)} c_{4,a}P_a^{sub} \tag{41}$$

where the first term in (41) is the construction cost for new distribution lines and the second term is the capacity expansion cost for PDN substations. If the existing substation on link $a \in C(i)$ has insufficient capacity to supply the additional EV charging stations, the expanded substation capacity is calculated as:

$$P_a^{sub} = \max\left\{0, P_a - P_{a,0}^{sub}\right\}, a \in C(i) \tag{42}$$

C. Coordinated Planning Constraints

1) TN Constraints: The coordinated planning model must satisfy the TN constraints:

$$Cons{-}\text{TN} = \left\{c_a = c_a^0 + n_a^c \Delta c_a, (27){-}(30), (37)\right\} \tag{43}$$

where the first constraint is the expanded road capacity; (27)–(30) are location constraints for EV charging stations in the UE traffic pattern; (37) states the interface between TN and PDN.

2) PDN Constraints: The PDN operation constraint is:

$$Cons{-}\text{PDN} = \begin{Bmatrix} v_j = v_i - (r_{ij}p_{ij} + x_{ij}q_{ij})/[v_1(1+n_{ij})], (34){-}(35), \\ \underline{v}_i \le v_i \le \bar{v}_i, 0 \le p_{ij} \le (1+n_{ij})\bar{p}_{ij}, i \in \mathbf{D_N}, (i,j) \in \mathbf{D_A} \end{Bmatrix} \tag{44}$$

where the first row gives the linearized DistFlow constraints; the second row includes voltage magnitude boundaries of nodes and active power flow bounds of distribution lines.

Accordingly, the traffic flow x_a and possible delay λ_a are determined by UTAM (27). The coordinated planning model (38)–(39) represents a challenging optimization problem. We discuss in Section IV the MILP enhancement of the planning model which is easily extended to multiple traffic and power demand scenarios and time horizons. We assume a fixed demand and a single period in the basic version of the planning model.

IV. MILP Enhancement for Coordinated Planning

This section provides a coordinated MILP planning model for coupled traffic-electric networks. There are three bottlenecks in (39)–(41) for solving the stated problem efficiently:

1) Nonlinear driving range logic constraints (28), UTAM (27), and interface between TN and PDN (37);

Authorized licensed use limited to: Washington State University. Downloaded on April 22,2021 at 20:11:05 UTC from IEEE Xplore. Restrictions apply.

2) Nonlinear term $\lambda_a x_a$ in C_{TN} and P_a^{sub} in C_{PDN};
3) Voltage drop equation as the first term in the first line of *Cons*-PDN.

Accordingly, equivalent linear versions are derived as follows.

A. Linearizing UTAM and Driving Range Logic Constraints

The feasible solution of (12)–(15) is the UE of TN because the NdP-SO (3)–(7) is an LP and the UTAM gives the corresponding primal-dual optimality condition [25]. (27) can be replaced by:

$$\begin{cases} \sum_k f_k^{rs} - q_{rs} = 0, \sum_k f_k^{rs}\delta_{ak}^{rs} - c_a \le 0, f_k^{rs} \ge 0, \\ \lambda_a \ge 0, \mu_a - \lambda_a = t_a^0, \pi_{rs} - \sum_a \sum_k \delta_{ak}^{rs}\mu_a \le 0, \\ \sum_{rs} \pi_{rs} q_{rs} - \sum_a \lambda_a c_a = \sum_{rs}\sum_a \sum_k f_k^{rs}\delta_{ak}^{rs} t_a^0, \\ a \in \mathbf{T_A}, k \in \mathbf{K_{rs}}, rs \in \mathbf{OD} \end{cases} \tag{45}$$

Considering (43), nonlinearities exist in $s_b SOC_a^k$ shown in (23), $\lambda_a c_a = \lambda_a(c_a^0 + n_a^c \Delta c_a)$ in (45) and $s_a x_a$ in (37). The first nonlinear term involves the production of a binary and a positive continuous variable. Here, a new variable $\xi_a^k = s_b SOC_a^k$ is introduced, which is linearized as:

$$\begin{cases} 0 \le \xi_a^k \le M_1 s_b \\ 0 \le SOC_a^k - \xi_a^k \le M_1(1 - s_b) \end{cases}, a \in \mathbf{\Gamma_k^{-1}}, b \in \mathbf{\Gamma_k}, k \in \mathbf{K_{rs}} \tag{46}$$

where M_1 is the big M value whose tightest value is the upper bound of SOC_a^k, i.e., 1. Accordingly, we express the linearized driving range logic constraints as

$$Cons-\mathrm{DRL}-\mathrm{Lin} = \begin{Bmatrix} SOC_b^k = SOC_a^k + s_b - (d_a + d_b)(1 - s_b)/2R - \xi_a^k, \\ 0 \le SOC_a^k - \xi_a^k \le M_1(1 - s_b), 0 \le \xi_a^k \le M_1 s_b, \\ (21)-(22), (24)-(25), a \in \mathbf{\Gamma_k^{-1}}, b \in \mathbf{\Gamma_k}, k \in \mathbf{K_{rs}} \end{Bmatrix} \tag{47}$$

The second nonlinear term $\lambda_a c_a$ represents the multiplication of integer and continuous variables. We introduce binary variables $z_{an}^c, n = 1, 2, \ldots, N_a^c$, in which

$$n_a^c = \sum_{n=1}^{N_a^c} z_{an}^c \tag{48}$$

Then, we have $\lambda_a c_a = \lambda_a c_a^0 (1 + \omega_c \sum_{n=1}^{N_a^c} z_{an}^c)$. Similar to (46), the nonlinear term $\xi_{an}^c = \lambda_a z_{an}^c$ is linearized as:

$$\begin{cases} 0 \le \xi_{an}^c \le M_2 z_{an}^c \\ 0 \le \lambda_a - \xi_{an}^c \le M_2(1 - z_{an}^c) \end{cases}, a \in \mathbf{T_A}, n = 1, 2, \ldots, N_a^c \tag{49}$$

where M_2 is the big M value with a possible value of the maximum link delay estimated from certain cases. The linearized UTAM constraints are reformulated as:

$$Cons-\mathrm{UTAM}-\mathrm{Lin} = \begin{Bmatrix} \sum_k f_k^{rs} = q_{rs}, \sum_k f_k^{rs}\delta_{ak}^{rs} \le c_a^0(1 + \omega_c \sum_{n=1}^{N_a^c} z_{an}^c), \\ f_k^{rs} \ge 0 \\ \lambda_a \ge 0, \mu_a - \lambda_a = t_a^0, \pi_{rs} - \sum_a \sum_k \delta_{ak}^{rs}\mu_a \le 0 \\ \sum_{rs}(\pi_{rs} q_{rs} - \sum_a \sum_k f_k^{rs}\delta_{ak}^{rs} t_a^0) \\ = \sum_a c_a^0(\lambda_a + \omega_c \sum_{n=1}^{N_a^c} \xi_{an}^c) \\ 0 \le \xi_{an}^c \le M_2 z_{an}^c, 0 \le \lambda_a - \xi_{an}^c \le M_2(1 - z_{an}^c) \\ a \in \mathbf{T_A}, k \in \mathbf{K_{rs}}, rs \in \mathbf{OD}, n = 1, 2, \ldots, N_a^c \end{Bmatrix} \tag{50}$$

The third nonlinear term $\xi_a = s_a x_a$ is linearized similar to the first nonlinear term $s_b SOC_a^k$, and (37) are replaced by

$$\begin{cases} P_i = P_i^d + \eta \sum_{a \in C(i)} \xi_a, 0 \le \xi_a \le M_3 s_a, \\ 0 \le x_a - \xi_a \le M_3(1 - s_a), i \in \mathbf{D_N}, a \in C(i) \end{cases} \tag{51}$$

where M_3 is the big M value whose value is the maximum link traffic flow estimated from certain cases. Thus, linearized TN constraints are reformulated as:

$$Cons-\mathrm{TN}-\mathrm{Lin} = \{Cons-\mathrm{DRL}-\mathrm{Lin}; Cons-\mathrm{UTAM} - \mathrm{Lin}; (29)-(30); (51)\} \tag{52}$$

B. Linearizing C_{TN} and C_{PDN}

The nonlinear term $\lambda_a x_a$ in C_{TN} includes two continuous variables and there is no general method to linearize this term without exploiting some approximation. The exact linear reformulation is derived based on the KKT conditions applied to UTAM. Considering the inequality constraint and its dual variable, we have

$$\lambda_a(x_a - c_a) = 0 \Rightarrow \lambda_a x_a = \lambda_a c_a \tag{53}$$

Combining with (48), C_{TN} is converted into a linear form, i.e.,

$$C_{TN} = \sum_{a \in \mathbf{T_A}} (c_{1,a} s_a + c_{2,a} y_a + c_{3,a} n_a^c + \omega t_a^0 x_a) + \sum_{a \in \mathbf{T_A}} \omega c_a^0 \left(\lambda_a + \omega_c \sum_{n=1}^{N_a^c} \xi_{an}^c\right) \tag{54}$$

The C_{TN} expressions in (40) and (54) are exact. The max function P_a^{sub} in (41) and (42) is reformulated as follows.

$$\begin{cases} P_a^{sub} \ge P_a - P_{a,0}^{sub}, P_a^{sub} \ge 0, \delta(P_a - P_{a,0}^{sub}) \\ \quad \ge P_a^{sub}, \delta(P_a - P_{a,0}^{sub}) \ge 0, \\ (1 - \delta)(P_a - P_{a,0}^{sub}) \le P_a^{sub}, (1 - \delta)(P_a - P_{a,0}^{sub}) \\ \quad \le 0, a \in C(i) \end{cases} \tag{55}$$

where δ is a newly introduced binary variable. We use a similar method to linearize δP_a, and obtain linearized C_{PDN}.

Authorized licensed use limited to: Washington State University. Downloaded on April 22,2021 at 20:11:05 UTC from IEEE Xplore. Restrictions apply.

C. Linearizing Voltage Drop Constraint

We multiply both sides of the first term in *Cons*-PDN (43) by $(1+n_{ij})$ and obtain:

$$v_j(1+n_{ij}) = v_i(1+n_{ij}) - (r_{ij}p_{ij} + x_{ij}q_{ij})/v_1, (i,j) \in \mathbf{D_A} \tag{56}$$

The nonlinear terms $v_i n_{ij}$ and $v_j n_{ij}$ include the multiplication of an integer and a continuous variable, which is similar to that of the second nonlinear term in Section IV-A. By introducing new binary variables $z_{ij}^n, n = 1, 2, \ldots, N_{ij}$ which satisfy:

$$n_{ij} = \sum_{n=1}^{N_{ij}} z_{ij}^n \tag{57}$$

we similarly linearize $\xi_{ij}^{n1} = v_j z_{ij}^n$ and $\xi_{ij}^{n2} = v_i z_{ij}^n$ as:

$$\begin{cases} v_j + \sum_{n=1}^{N_{ij}} \xi_{ij}^1 = v_i + \sum_{n=1}^{N_{ij}} \xi_{ij}^2 - (r_{ij}p_{ij} + x_{ij}q_{ij})/v_1, \\ 0 \le \xi_{ij}^{n1} \le \bar{v}_j z_{ij}^n, 0 \le v_j - \xi_{ij}^{n1} \le \bar{v}_j(1 - z_{ij}^n), 0 \\ \quad \le \xi_{ij}^{n2} \le \bar{v}_i z_{ij}^n, \\ 0 \le v_i - \xi_{ij}^{n1} \le \bar{v}_i(1 - z_{ij}^n), (i,j) \in \mathbf{D_A}, a \in \mathbf{T_A}, \\ \quad \times n = 1, 2, \ldots, N_{ij} \end{cases} \tag{58}$$

Accordingly, we express the linearized PDN constraints as

$$Cons-\text{PDN} - \text{Lin} = \left\{ \begin{matrix} \underline{v}_i \le v_i \le \bar{v}_i, 0 \le p_{ij} \le (1+n_{ij})\bar{p}_{ij}, \\ (34)-(35), (58), i \in \mathbf{D_N}, (i,j) \in \mathbf{D_A} \end{matrix} \right\} \tag{59}$$

If the integrality of binary variable is relaxed, *Cons*-PDN-Lin yields linear constraints.

D. Final MILP Formulation

The coordinated MILP planning model for the coupled traffic-electric networks is stated as:

$$\begin{matrix} \min & C_{TN} + C_{PDN} \\ \text{s.t.} & \{Cons-\text{TN} - \text{Lin}; Cons-\text{PDN} - \text{Lin}\} \end{matrix} \tag{60}$$

where C_{TN} and C_{PDN} are stated in (54) and (55), respectively; *Cons*-TN-Lin and *Cons*-PDN-Lin are stated in (52) and (59).

The MILP enhancement of the planning problem relies on linear models of ECSLM and PDN. Since network radiality is crucial for voltage drop (36), the linearized DistFlow model (44) and (59) is only applicable in a radial PDN. In engineering practices, PDNs are intentionally operated with a radial topology. However, in a weakly meshed PDN, the proposed MILP coordinated planning model is still applicable by determining power flow directions in advance [25]. Also, the proposed model helps make planning decisions on coupled traffic-electric networks to reduce the traffic congestion and enhance the sustainable operation of smart cities.

So far, the coordinated planning model in Section III has been transformed into a MILP model without approximation error involved. The formulated MILP model can be readily solved to calculate the global optimality by a variety of optimization software, such as GAMS, CPLEX, GUROB, etc. Mathematically,

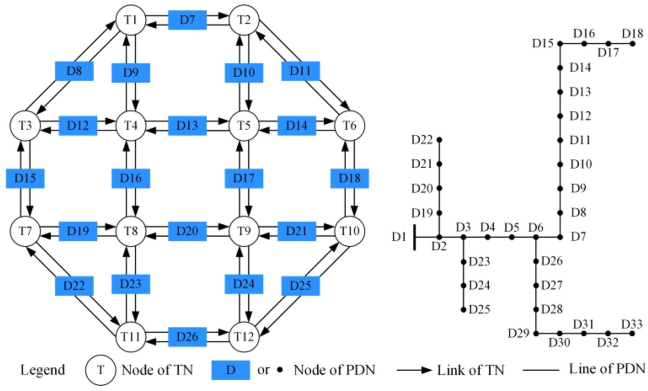

Fig. 3. Topology of coupled traffic-electric networks.

the rationality of the constraint coefficients is the sufficient condition for the existence of optimal solution to a mixed-integer programming problem [34].

Here a simple proof for existence of optimal solution to the MILP model is introduced and details refer to [34]. For a general MILP model:

$$[\text{MILP}_1] \quad \begin{matrix} \min & \mathbf{c_1^T x} + \mathbf{c_2^T y} \\ \text{s.t.} & \mathbf{A_1 x} + \mathbf{A_2 y} = \mathbf{beq}, \\ & \mathbf{A_3 x} + \mathbf{A_4 y} \le \mathbf{b}, \\ & \mathbf{x} \ge \mathbf{0}, \mathbf{y} \ge \mathbf{0}, \mathbf{x}\ integer. \end{matrix} \tag{61}$$

where $\mathbf{x}$ and $\mathbf{y}$ are vectors of integer and continuous decision variables, respectively; $\mathbf{c_1}$, $\mathbf{c_2}$, $\mathbf{A_1}$, $\mathbf{A_2}$, $\mathbf{beq}$, $\mathbf{A_3}$, $\mathbf{A_4}$ and $\mathbf{b}$ are vectors and matrices of sizes $(n_1 \times 1)$, $(n_2 \times 1)$, $(m_1 \times n_1)$, $(m_1 \times n_2)$, $(m_1 \times 1)$, $(m_2 \times n_1)$, $(m_2 \times n_2)$ and $(m_2 \times 1)$ respectively. Inequality constraints in (60) can be transferred into equality constraints by introducing integer and continuous slack variables. The convex hull of the feasible region is denoted as $\mathbf{C_m}$. According to Theorem 3.9 in [34], if $\mathbf{A_1}$, $\mathbf{A_2}$, $\mathbf{A_3}$ and $\mathbf{A_4}$ are rational, then $\mathbf{C_m}$ is polyhedral (i.e., the intersection of a finite number of half-spaces). Then, MILP$_2$, which is denoted by replacing the feasible region of MILP$_1$ by $(\mathbf{x}, \mathbf{y}) \in \mathbf{C_m}$, becomes a linear programming problem. Hence, if MILP$_2$ is feasible and bounded, there must be an optimal solution $(\mathbf{x}^*, \mathbf{y}^*)$ at some extreme point of $\mathbf{C_m}$. Based on Lemma 3.1 in [34], $(\mathbf{x}^*, \mathbf{y}^*)$ also belongs to the feasible region of MILP$_1$. In the case that **beq** and **b** are also rational, readers can refer to [35]. All constraint coefficients of the feasible and bounded MILP model in Section IV are rational numbers, which indicates the optimal solution exists. Moreover, the solvers in GAMS [36] ensure the optimality of the MILP model.

V. Case Studies

A. Case Overview and Basic Settings

We consider a 12-node TN highway [2] coupled with IEEE 33-node PDN [37] to illustrate the proposed planning method. In Fig. 3, the 12-node TN and the IEEE 33-node PDN are depicted on left and right sides, respectively. The TN nodes are denoted by circles and numbered by T1, T2, ..., T12; the PDN nodes

Authorized licensed use limited to: Washington State University. Downloaded on April 22,2021 at 20:11:05 UTC from IEEE Xplore. Restrictions apply.

TABLE I
PARAMETERS OF TN LINKS

No.	Link	c_a (p.u.)	t_a^0 (h)	d_a (km)	$c_{3,a}$ (10^3\$)
1	T1-T2	20	0.6	60	200
2	T1-T3	18	0.3	30	75
3	T2-T6	17	0.4	40	125
4	T1-T4	9.8	0.2	20	50
5	T2-T5	7.9	0.3	30	80
6	T3-T4	8.5	0.3	30	85
7	T4-T5	13.5	0.8	80	225
8	T5-T6	8.2	0.4	40	100
9	T3-T7	19	0.6	60	175
10	T4-T8	14	0.7	70	185
11	T5-T9	13.8	0.8	80	230
12	T6-T10	20	0.6	60	190
13	T7-T8	8.9	0.3	30	70
14	T8-T9	13.2	0.7	70	185
15	T9-T10	9.15	0.3	30	75
16	T7-T11	17.5	0.3	30	90
17	T8-T11	9.76	0.2	20	50
18	T9-T12	8.97	0.2	20	50
19	T12-T10	18.2	0.3	30	75
20	T11-T12	20	0.5	50	200

TABLE II
O-D PAIRS AND TRAVEL RATES IN TN

O-D pair	q_{rs} (p.u.)	O-D pair	q_{rs} (p.u.)	O-D pair	q_{rs} (p.u.)
T1-T6	12	T3-T6	12	T4-T9	4
T1-T10	16	T3-T10	16	T4-T10	8
T1-T11	12	T3-T11	9.6	T4-T12	12
T1-T12	8	T3-T12	6.4	-	-

are represented by blue blocks in the TN part and black spots in the PDN part, and numbered by D1, D2, . . . , D33. The nodal coupling of the two networks is shown in the TN part of Fig. 3. According to [2], the parameters of TN links are listed in Table I. In our case, the traffic leaves from the northwest and travels to the east and the south. Details of the O-D pairs and their trip rates are provided in Table II [25].

In PDN, D1 is the reference node which is connected to the main grid. The PDN parameters are provided in Table A-2 of [29]. The line number is the downstream node number minus one. Lower and upper bounds of nodal voltage magnitude are $\underline{v}_i = 0.95$ and $\bar{v}_i = 1.05$, respectively, the voltage magnitude at the reference node is $v_1 = 1.05$, and active power flow limits are set at original active power flows. The per-unit cost of a distribution line is $c_{ij} = \$3 \times 10^5$ [25]. $P_{a,0}^{sub}$ is equal to the corresponding constant demand.

Referring to parameter settings in [10], [12] and [25], the rest of the system parameters are given as follows. The cost of a new EV charging station is $c_{1,a} = \$1.63 \times 10^5$. The cost of a charging spot $c_{2,a}$ is \$3,160. The cost of substation capacity expansion $c_{4,a}$ is 5,000 \$/kVA. The monetary value of travel time in TN is $\omega = \$10^4$. The maximum number of charging spots is $\bar{y}_a = 200$. The driving range of EVs with full charge is $R = 100$ km. The arrival and departure SOC (SOC_O and SOC_D) are both set at 0.5. The upper bounds of lanes N_a^c and distribution lines N_{ij} that can be expanded are set at 10 and 5, respectively. The charging rate of TN traffic flow is $\eta = 0.3$. All

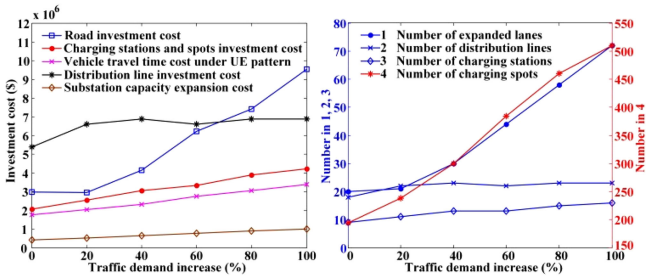

Fig. 4. Investment costs and coordinated planning results.

TABLE III
EXPANSION STRATEGIES OF TN LINKS

No.	Traffic demand increase (%)						No.	Traffic demand increase (%)					
	0	20	40	60	80	100		0	20	40	60	80	100
1	4	4	4	4	4	4	11	1	0	0	1	0	4
2	1	1	1	3	1	0	12	3	1	1	1	3	1
3	5	4	4	5	5	5	13	1	0	0	0	0	2
4	0	0	0	0	9	6	14	0	0	1	4	0	2
5	0	0	0	0	0	0	15	0	1	3	7	1	7
6	0	0	0	3	0	4	16	0	4	4	4	3	3
7	2	0	0	2	5	6	17	2	0	3	0	8	9
8	0	0	0	0	6	3	18	1	1	0	0	0	0
9	0	3	4	4	3	5	19	0	0	0	0	0	0
10	0	1	3	5	6	7	20	0	1	2	1	4	4

TABLE IV
PARTIAL EXPANSION STRATEGIES OF DISTRIBUTION LINES IN PDN

No.	Line	Traffic demand increase (%)					
		0	20	40	60	80	100
18	D2-D19	0	1	1	1	1	1
19	D19-D20	0	1	1	1	1	1
20	D20-D21	0	1	1	1	1	1
21	D21-D22	0	1	1	1	1	1
22	D3-D23	1	0	1	0	1	1
25	D6-D26	0	1	1	1	1	1

simulations are implemented on a computer with Intel i7-6700T CPU and 8-GB memory using GAMS 24.1.3 [36].

B. Coordinated Planning Results and Analysis

The coordinated planning model (61) for the coupled traffic-electric networks is solved using 6 traffic demand scenarios. The reference traffic demand is listed in Table II. In each scenario, travel rates of all O-D pairs are increased proportionally. In these 6 scenarios, parameter q_{rs} is increased by 0%, 20%, 40%, 60%, 80% and 100%, respectively. Fig. 4 depicts the corresponding investment costs. Also, Tables III–IV show the optimal expansion planning strategies of TN links and PDS distribution lines in different traffic demand scenarios. The optimal locations of EV charging stations with corresponding numbers of charging spots are listed in Table V.

In Table III, roads are expanded when the traffic flow increases. Although, the optimal expansion number for each TN road is not monotonically increasing with the growing traffic, as per-unit costs of newly expanded lanes and traffic flows on various links are quite different.

The expansion strategies for distribution lines 18 through 22 and 25 in traffic demand scenarios are listed in Table IV. The expansion strategies for distribution lines 1 through 17 are not listed in Table IV because they all follow the same pattern (i.e.,

Authorized licensed use limited to: Washington State University. Downloaded on April 22,2021 at 20:11:05 UTC from IEEE Xplore. Restrictions apply.

TABLE V
STATION LOCATIONS AND CORRESPONDING NUMBER OF CHARGING SPOTS

No.	Traffic demand increase (%)						No.	Traffic demand increase (%)					
	0	20	40	60	80	100		0	20	40	60	80	100
1	50	49	49	50	50	50	11	11	4	4	7	3	24
2	16	15	15	28	14	0	12	33	20	15	20	40	20
3	49	41	41	50	50	49	13	0	0	0	0	0	7
4	0	0	0	0	40	29	14	0	2	10	30	4	13
5	0	0	0	0	0	0	15	0	0	11	31	3	30
6	0	0	0	11	0	15	16	0	36	37	43	32	34
7	17	4	4	14	36	42	17	9	0	14	0	39	44
8	0	0	0	0	23	9	18	0	0	0	0	0	0
9	9	36	45	47	38	50	19	0	0	0	0	0	0
10	0	11	25	35	46	50	20	0	20	30	18	42	44

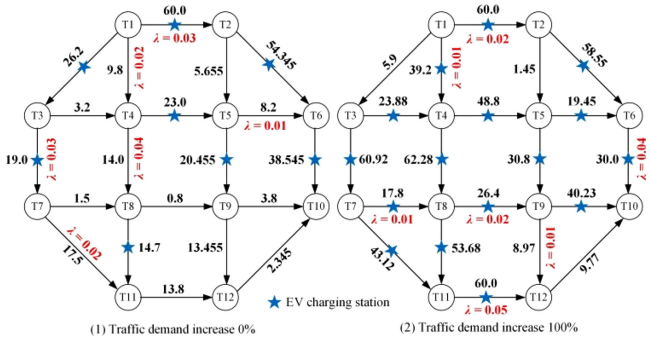

Fig. 5. Distribution of traffic flows at UE and EV locations of charging stations.

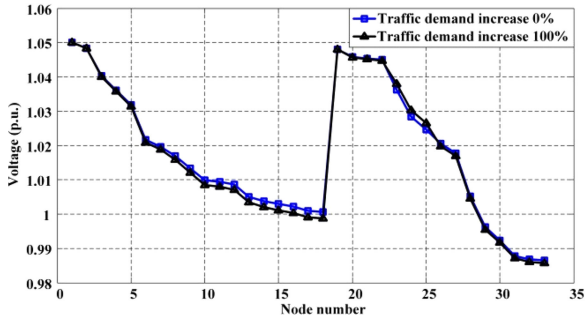

Fig. 6. Voltage profiles under different traffic increase scenarios.

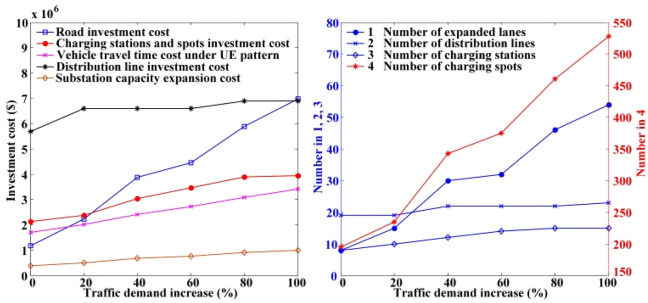

Fig. 7. Investment costs with high link capacity.

add 1 line in parallel with existing lines) in the 6 traffic demand scenarios. In this case, distribution lines 23, 24 and 26 through 32 are not expanded.

In Table V, the total number of charging spots grows in higher traffics, as expected. Meanwhile, Fig. 4 illustrates the growing trend in investment cost and component expansion pertaining to traffic scenarios, which shows the dominant scenario for investment on roads and distribution lines. In our cases, both TN and PDN operation constraints are feasible and traffic and EV charging demands will be satisfied as sufficient TN roads and PDN lines are expanded.

Fig. 5 depicts the locations of EV charging stations and the traffic flow on each UE pattern link for traffic increase scenarios of 0% and 100%. The expansion of distribution lines in the 0% traffic increase scenario can serve additional charging demands at buses D7, D9, D12, D14, D15 and D16 in the 100% traffic increase scenario. Moreover, links T7-T8, T8-T9, T9-T10, T7-T11, T8-T11 and T5-T6 carry heavier traffics in 100% traffic increase scenario, leading to higher charging demands at buses D19 through D23 and D26. In this regard, distribution lines D2-D19, D19-D20, D20-D21, D21-D22, D3-D23 and D6-D26 are upgraded with a higher priority to ensure continuous power deliveries to these buses.

Fig. 6 demonstrates the PDN bus voltages for traffic increase scenarios of 0% and 100%. Here, all bus voltages are within the specified range which indicates that the PDN operation is secure in the 100% traffic increase scenario after distribution line expansion. In Table IV, although the traffic is increased from 20% to 100%, the PDN expansion strategies are almost the same, representing a social optimal perspective. This result shows the importance of considering the interdependence of TN and PDN in infrastructural planning.

C. Sensitivity Analyses

We consider the following cases for sensitivity analyses.

1) Link Capacity Constraints: Fig. 7 shows the results as we increase the capacity of each link by 20%. When the link capacities are increased, fewer lanes are to be expanded on existing roads as the traffic grows. This sensitivity analysis provides a roadmap for planning road upgrades.
2) Driving Range after Full Charge: EV driving range will increase with advancing the battery technology. By then there will be various types of EVs with different driving ranges. Note that the driving range constraints become stricter as the driving range decreases. Hence, if the EVs with the smallest driving range can travel through TN without running out of energy, then the ones with larger driving range will also succeed. Accordingly, 7 different driving range scenarios are assumed, i.e., R = 100 km, 150 km, 200 km, 250 km, 300 km, 350 km and 400 km. The total cost and the number of charging stations in various EV driving range scenarios are shown in Fig. 8. Here, the total cost and the required number of charging stations will decrease with increasing the EV driving range. In the test network, an EV charging station will not be necessary when the driving range is longer than 300 km.
3) *SOC* Effect: SOC_O and SOC_D affect the siting and the sizing of EV charging stations. Fig. 9 shows the total investment cost using different SOC_O and SOC_D values. The figure demonstrates that the total investment cost is monotonically decreasing with increasing SOC_O.

Authorized licensed use limited to: Washington State University. Downloaded on April 22,2021 at 20:11:05 UTC from IEEE Xplore. Restrictions apply.

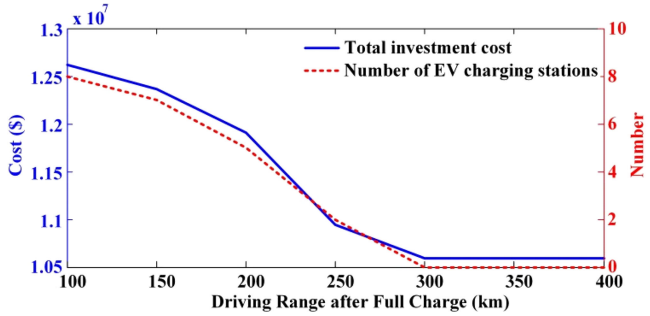

Fig. 8. Influence of driving range after full charge.

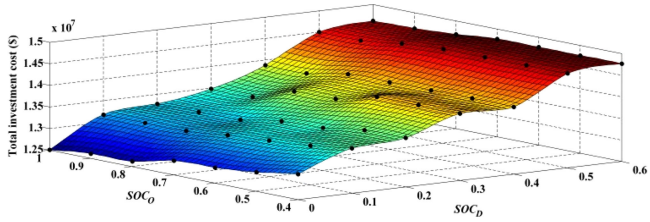

Fig. 9. Influence of *SOC*.

TABLE VI
EXPECTED TOTAL INVESTMENT COST CONSIDERING UNCERTAINTIES OF SOC_O AND SOC_D ($\times 10^2$ \$)

σ_1 \ σ_2	0.05	0.10	0.15	0.20	0.25	0.30	0.35
0.05	138265	138160	138281	138295	138263	138221	138180
0.10	138228	138136	138217	138226	138168	138113	138062
0.15	138133	138042	138145	138148	138099	138045	137994
0.20	138019	137969	138093	138100	138058	138006	137957
0.25	137936	137918	138057	138070	138032	137982	137935
0.30	137875	137880	138032	138050	138015	137967	137921
0.35	137829	137853	138013	138036	138003	137956	137910

Conversely, higher SOC_D leads to a higher investment cost. In practice, these two indices are obtained by investigating the EV charging behavior in TN. Moreover, a scenario-based stochastic optimization method [38] is used to consider the *SOC* uncertainties. Table VI lists the expected total investment cost for different σ_1 and σ_2 when SOC_O and SOC_D are assumed to obey normal distributions N (0.7, σ_1) and N (0.3, σ_2), respectively. For a fixed σ_1, the total investment cost is essentially the same when σ_2 increases from 0.05 to 0.35. The same conclusion can be drawn for a fixed σ_2. In practice, *SOC* uncertainties have a minute effect on the total investment cost.

4) Charging rate η: Charging the traffic flow rate affects the charging demand in an EV charging station. Fig. 10 shows the investment cost when charging rate η increases from 0.1 to 1. The figure demonstrates that the expansion strategies of TN links and the traffic flow distribution in TN are the same for different charging rate scenarios. EV charging request increases linearly as the charging rate grows linearly. Hence, investment costs for charging stations and spots, substation capacity expansion cost, and the number of charging spots increase linearly with linearly increasing charging rates.

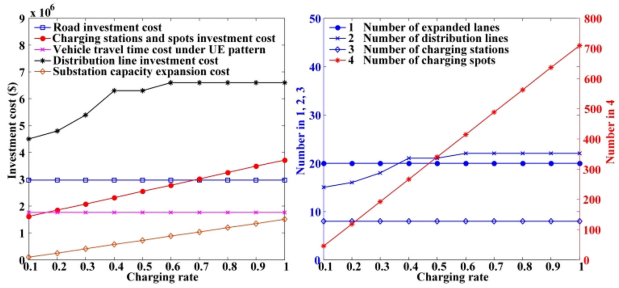

Fig. 10. Influence of charging rate η.

TABLE VII
COMPUTATION PERFORMANCE IN DIFFERENT COUPLED NETWORKS

System		Traffic demand increase (%)				
		0	20	40	60	100
CPU time (s)	Network 1	1.49	1.51	1.67	1.86	2.26
	Network 2	7.38	10.61	15.85	23.89	36.19
Iteration number	Network 1	46	54	68	92	128
	Network 2	152	227	316	438	715

D. Computation Performance

We have performed additional numerical experiments and presented the results in Section IV-D in the revised manuscript. These tests are carried out to present the computation performance of the proposed MILP model using GAMS 24.1.3. The original coupled network (i.e., a 12-node TN coupled with an IEEE 33-node PDN in Fig. 3) is referred to as the coupled network 1. We consider a larger scale system, referred to as the coupled network 2, which includes 4 12-node TNs coupled with an IEEE 123-node PDN. Similar to the nodal coupling of the two networks shown in the TN part of Fig. 3, the edges of the 4 TNs are coupled using D11-D30, D31-D50, D51-D70 and D71-D90 in the IEEE 123-node PDN, respectively. Table VII shows the CPU times and iteration numbers for the two coupled networks.

It is seen that CPU time increases as the traffic demand grows. Also, proposed tests on larger scale network will cost more CPU time. Nevertheless, the MILP models of all cases are solved in less than 1 minute and the calculation burden in all cases is within an acceptable range for a planning problem. In essence, we have proposed a coordinated MILP planning model that is feasible for the coupled traffic-electric network and can obtain the best solution in a reasonable pre-specified time limit.

VI. CONCLUSION

This paper studies the coordinated planning of EV charging stations and the coupled traffic-electric networks. UTAM is proposed to simulate realistic traffic flows in TN, and the NdP model and the primal-dual optimality condition is employed to overcome the shortcomings of the conventional BPR function when road capacity is a variable. Moreover, incorporating EV driving range and UTAM-based traffic flow equilibrium, ECSLM is introduced to estimate EV charging demands. For simplicity, a linear function is used to model each charging station's serviceability. In PDN with a radial topology, the linearized DistFlow model is applied to calculate bus voltage magnitudes and distribution line power flows. A MILP model is developed for the coordi-

Authorized licensed use limited to: Washington State University. Downloaded on April 22,2021 at 20:11:05 UTC from IEEE Xplore. Restrictions apply.

nated planning model of the coupled traffic-electric networks. Numerical experiments illustrate that the proposed approach can provide a global optimal planning solution for coupled traffic-electric networks with reasonable computation efforts.

REFERENCES

[1] M. Ehsani, Y. Gao, and A. Emadi, *Modern Electric, Hybrid Electric, and Fuel Cell Vehicles: Fundamentals, Theory, and Design*. Boca Raton, FL, USA: ROC Press, 2018.

[2] W. Wei, S. Mei, L. Wu, J. Wang, and Y. Fang, "Robust operation of distribution networks coupled with urban transportation infrastructures," *IEEE Trans. Power Syst.*, vol. 32, no. 3, pp. 2118–2130, May 2017.

[3] M. E. Khodayar, L. Wu, and M. Shahidehpour, "Hourly coordination of electric vehicle operation and volatile wind power generation in SCUC," *IEEE Trans. Smart Grid*, vol. 3, no. 3, pp. 1271–1279, Sep. 2012.

[4] S. D. Manshadi, M. E. Khodayar, K. Abdelghany, and H. Uster, "Wireless charging of electric vehicles in electricity and transportation networks," *IEEE Trans. Smart Grid*, vol. 9, no. 5, pp. 4503–4512, Sep. 2018.

[5] Z. Liu, F. Wen, and G. Ledwich, "Optimal planning of electric-vehicle charging stations in distribution systems," *IEEE Trans. Power Del.*, vol. 28, no. 1, pp. 102–110, Jan. 2013.

[6] Y. Zheng, Z. Dong, Y. Xu, K. Meng, J. Zhao, and J. Qiu, "Electric vehicle battery charging/swap stations in distribution systems: comparison study and optimal planning," *IEEE Trans. Power Syst.*, vol. 29, no. 1, pp. 221–229, Jan. 2014.

[7] W. Yao *et al.*, "A multi-objective collaborative planning strategy for integrated power distribution and electric vehicle charging systems," *IEEE Trans. Power Syst.*, vol. 29, no. 4, pp. 1811–1821, Jul. 2014.

[8] H. Zhang, S. Moura, Z. Hu, W. Qi, and Y. Song, "A second order cone programming model for planning PEV fast-charging stations," *IEEE Trans. Power Syst.*, vol. 33, no. 3, pp. 2763–2777, May 2018.

[9] S. Wang, Z. Dong, F. Luo, K. Meng, and Y. Zhang, "Stochastic collaborative planning of electric vehicle charging stations and power distribution system," *IEEE Trans. Ind. Informat.*, vol. 14, no. 1, pp. 321–331, Jan. 2018.

[10] H. Zhang, Z. Hu, Z. Xu, and Y. Song, "An integrated planning framework for different types of PEV charging facilities in urban area," *IEEE Trans. Smart Grid*, vol. 7, no. 5, pp. 2273–2284, Sep. 2016.

[11] N. Shahraki, H. Cai, M. Turkay, and M. Xu, "Optimal locations of electric public charging stations using real world vehicle travel patterns," *Transp. Res. D, Tr. E.*, vol. 41, pp. 165–176, Dec. 2015.

[12] H. Zhang, S. Moura, Z. Hu, and Y. Song, "PEV fast-charging station siting and sizing on coupled transportation and power networks," *IEEE Trans. Smart Grid*, vol. 9, no. 4, pp. 2595–2605, Jul. 2018.

[13] S. Li, Y. Huang, and S. J. Mason, "A multi-period optimization model for the deployment of public electric vehicle charging stations on network," *Transp. Res. C, Technol.*, vol. 65, pp. 128–143, Apr. 2016.

[14] Z. Li, M. Shahidehpour, S. Bahramirad, and A. Khodaei, "Optimizing traffic signal settings in smart cities," *IEEE Trans. Smart Grid*, vol. 8, no. 5, pp. 2382–2393, Sep. 2017.

[15] W. Wei, L. Wu, J. Wang, and S. Mei, "Network equilibrium of coupled transportation and power distribution systems," *IEEE Trans. Smart Grid*, vol. 9, no. 6, pp. 6764–6779, Nov. 2018.

[16] W. Wei, S. Mei, L. Wu, M. Shahidehpour, and Y. Fang, "Optimal traffic-power flow in urban electrified transportation networks," *IEEE Trans. Smart Grid*, vol. 8, no. 1, pp. 84–95, Jan. 2017.

[17] H. Zhang, S. J. Moura, Z. Hu, W. Qi, and Y. Song, "Joint PEV charging network and distributed PV generation planning based on accelerated generalized benders decomposition," *IEEE Trans. Transp. Electrification*, vol. 4, no. 3, pp. 789–803, Sep. 2018.

[18] M. Alizadeh, H. Wai, M. Chowdhury, A. Goldsmith, A. Scaglione, and T. Javidi, "Optimal pricing to manage electric vehicles in coupled power and transportation networks," *IEEE Trans. Control Netw. Syst.*, vol. 4, no. 4, pp. 863–875, Dec. 2017.

[19] Y. Sun, Z. Li, M. Shahidehpour, and B. Ai, "Battery-based energy storage transportation for enhancing power system economics and security," *IEEE Trans. Smart Grid*, vol. 6, no. 5, pp. 2395–2402, Sep. 2015.

[20] K. Hou *et al.*, "A reliability assessment approach for integrated transportation and electrical power systems incorporating electric vehicles," *IEEE Trans. Smart Grid*, vol. 9, no. 1, pp. 88–100, Jan. 2018.

[21] X. Wang, M. Shahidehpour, C. Jiang, and Z. Li, "Resilience enhancement strategies for power distribution network coupled with urban transportation system," *IEEE Trans. Smart Grid*, to be published, doi: 10.1109/TSG.2018.2848970.

[22] F. Chudak, V. Eleuterio, and Y. Nesterov, "Static traffic assignment problem: A comparison between Beckmann (1956) and Nesterov & de Palma (1998) models," in *Proc. Swiss Transp. Res. Conf.*, Sep. 2007, pp. 1–23.

[23] Y. Nesterov and A. de Palma, "Stationary dynamic solutions in congested transportation networks: summary and perspectives," *Netw. Spatial Econ.*, vol. 3, no. 3, pp. 371–95, Sep. 2003.

[24] Y. Nesterov, "Stable traffic equilibria: Properties and applications," *Optim. Eng.*, vol. 1, no. 1, pp. 29–50, Jun. 2000.

[25] W. Wei, L. Wu, J. Wang, and S. Mei, "Expansion planning of urban electrified transportation networks: A mixed-integer convex programming approach," *IEEE Trans. Transp. Electrific.*, vol. 3, no. 1, pp. 210–224, Mar. 2017.

[26] Bureau of Public Roads, "*Traffic Assignment Manual*," U.S. Dept. of Commerce, Washington, DC, USA, 1964.

[27] T. Larsson and M. Patriksson, "An augmented lagrangean dual algorithm for link capacity side constrained traffic assignment problems," *Transp. Res. Part B, Methodological*, vol. 29, no. 6, pp. 433–455, Jan. 1995.

[28] J. G. Wardrop, "Some theoretical aspects of road traffic research," *Proc. Inst. Civil Eng.*, vol. 1, no. 3, pp. 325–362, May 1952.

[29] S. A. Mir Hassani and R. Ebrazi, "A flexible reformulation of the refueling station location problem," *Transp. Sci.*, vol. 47, no. 4, pp. 617–628, 2013.

[30] C. Upchurch, M. Kuby, and S. Lim, "A model for location of capacitated alternative-fuel stations," *Geogr. Anal.*, vol. 41, no. 1, pp. 127–148, 2009.

[31] X. Wang, Z. Li, M. Shahidehpour, and C. Jiang, "Robust line hardening strategies for improving the resilience of distribution systems with variable renewable resources," *IEEE Trans. Sustain. Energy*, vol. 10, no. 1, pp. 386–395, Jan. 2019.

[32] F. He, D. Wu, Y. Yin, and Y. Guan, "Optimal deployment of public charging stations for plug-in hybrid electric vehicles," *Transp. Res. B, Methodol.*, vol. 47, pp. 87–101, Jan. 2013.

[33] F. He, Y. Yin, J. Wang, and Y. Yang, "Sustainability SI: Optimal prices of electricity at public charging stations for plug-in electric vehicles," *Netw. Spatial Econ.*, vol. 16, no. 1, pp. 131–154, Mar. 2016.

[34] R. R. Meyer, "On the existence of optimal solutions to integer and mixed-integer programming problems," *Math. Program.*, vol. 7, no. 1, pp. 223–235, Dec. 1974.

[35] L. A. Wolsey, "Group theoretic results in mixed integer programming," *Operations Res.*, vol. 19, no. 7, pp. 1691–1697, Dec. 1971.

[36] GAMS 24.1.3, May 30, 2013. [Online]. Available: https://www.gams.com/download-old/

[37] M. Aman, G. Jasmon, A. Bakar, and H. Mokhlis, "A new approach for optimum simultaneous multi-DG distributed generation units placement and sizing based on maximization of system loadability using HPSO algorithm," *Energy*, vol. 66, pp. 202–215, Mar. 2014.

[38] L. Wu, M. Shahidehpour, and Z. Li, "Comparison of scenario-based and interval optimization approaches to stochastic SCUC," *IEEE Trans. Power Syst.*, vol. 27, no. 2, pp. 913–921, May 2012.

Xu Wang received the B.S. degree in electrical engineering from Southeast University, China, in 2010, and the Ph.D. degree from Shanghai Jiao Tong University, China, in 2016. He is currently an Assistant Professor with Shanghai Jiao Tong University, China, and also a Visiting Faculty in the Robert W. Galvin Center for Electricity Innovation at Illinois Institute of Technology (IIT), Chicago, USA. His research interests include electricity market, power flow calculation, and power system economics and optimization.

Mohammad Shahidehpour (F'01) is the University Distinguished Professor, and Bodine Chair Professor and Director of Robert W. Galvin Center for Electricity Innovation at IIT in Chicago, USA. Dr. Shahidehpour is a Member of the US National Academy of Engineering, Fellow of the American Association for the Advancement of Science (AAAS), and Fellow of the National Academy of Investors.

Chuanwen Jiang received the M.S. and Ph.D. degrees from Huazhong University of Science and Technology, Wuhan, China, in 1996 and 2000, respectively, and completed his postdoctoral research in Shanghai Jiao Tong University, China, in 2002. He is a Professor with the School of Electronic Information and Electrical Engineering, Shanghai Jiao Tong University. His research interests include reservoir dispatch, power system analysis, electricity markets, and power system economics and optimization.

Zhiyi Li (GSM'14–M'17) received the B.S. degree in electrical engineering from Xi'an Jiaotong University, Xi'an, China, in 2011, and the M.S. degree in electrical engineering from Zhejiang University, China, in 2014. He received the Ph.D. degree from the Department of Electrical and Computer Engineering Department, IIT, in 2017.

Authorized licensed use limited to: Washington State University. Downloaded on April 22,2021 at 20:11:05 UTC from IEEE Xplore. Restrictions apply.